JOURNAL OF GEOPHYSICAL RESEARCH, VOL. 104, NO. A8, PAGES 17,021–17,032, AUGUST 1, 1999

Electron velocity distribution functions from the solar wind to the corona

V. Pierrard
Institut d'Aéronomie Spatiale de Belgique, Brussels, Belgium

M. Maksimovic
Space Science Department, European Space Agency, European Space and Technology Center, Noordwijk, The Netherlands

J. Lemaire
Institut d'Aéronomie Spatiale de Belgique, Brussels, Belgium

Abstract. Typical electron velocity distribution functions observed at 1 AU from the Sun by the 3DP instrument onboard Wind are used as boundary conditions to determine the electron velocity distribution function at 4 solar radii in the corona. The velocity distribution functions (VDFs) at low altitude are obtained by solving the Fokker-Planck equation, using two different sets of boundary conditions. The first set typically corresponds to a VDF observed in a low-speed solar wind flow (i.e., characterized by "core" and "halo" electrons); the second one corresponds to high-speed solar wind (i.e., characterized by "core," "halo,", and "strahl" populations). We use the observed electron VDFs as test particles, which are submitted to external forces and Coulomb collisions with a background plasma. Closer to the Sun, the relative density of the core electrons is found to increase compared to the density of the halo population. Nevertheless, we find that in order to match the observed distributions at 1 AU, suprathermal tails have to be present in the VDF of the test electron at low altitudes in the corona.

1. Introduction

What is the origin of the shape of the electron velocity distribution functions (VDFs) observed in the solar wind? These VDFs exhibit, most of the time, three different components: a thermal core and a halo component, which are present at all pitch angles, and a sharply field aligned "strahl," which is present most often in the fast solar wind [*Feldman et al.*, 1975; *Rosenbauer et al.*, 1977; *Pilipp et al.*, 1987]. The core population conforms closely to a displaced Maxwellian distribution while, the hot population supports enhanced high energy tails that decrease as a power law of the energy. In the low-speed solar wind, the core and the halo are nearly isotropic and their mean velocities are close to the bulk speed. In the high-speed solar wind, the halo component is more anisotropic and exhibits larger drift velocities. The strahl is mainly present in the fast wind. It represents the anisotropic component of halo electrons that stream away from the Sun with a drift velocity aligned with the local magnetic field direction. The strahl's angular extension is observed to increase with the electron energy and the heliospheric distance [*Hammond et al.*, 1996].

Some authors have proposed kinetic models for the heat conduction in the solar wind acceleration regions and attempt to describe the origin of typical 1 AU electron VDFs [*Ogilvie and Scudder*, 1978; *Scudder and Olbert*, 1979a, b]. Superdiffusion processes have also been proposed to explain the suprathermal tails observed in many space plasmas [*Treumann*, 1997]. Nevertheless, the actual origin of the typical electron VDF shapes in the low-speed and high-speed solar wind is far from being understood. If the strahl population could be assumed to consist of energetic electrons escaping from the corona and being focused because of the magnetic moment conservation [*Schulz and Eviatar*, 1972; *Feldman et al.*, 1975], what about the symmetric halo component? Do these halo electrons have their origin in the corona, or are they due to other processes such as sophisticated wave-particle interactions or, for instance, large-scale interplanetary Corotating Interaction Region shock reflections? Recent studies point out that "velocity filtration" may be the source of high-energy electrons contributing to an enhanced heat flux [*Scudder*, 1992a, b]. In order to trace the origin of the shape of the electron VDF, it is useful to study its change from inside the corona to large radial distances from the Sun.

Paper number 1999JA900169..
0148-0227/99/1999JA900169$09.00

The evolution of the VDF with the radial distance contains information about the physical processes in the acceleration region.

In the present paper, we shed new light on this topic by studying a model with a test population of solar wind electrons submitted to Coulomb collisions with a background electron population assumed to be Maxwellian or Lorentzian. This model is an adaptation of a recent collisional model of the polar wind by *Pierrard and Lemaire* [1998]. These authors have studied the diffusion and upward bulk motion of H^+ ions through a background of O^+ ions in the Earth polar wind. Note that the present model has been greatly inspired and is very similar to the *Lie-Svendsen et al.* [1997] model but with alternative boundary conditions and distributions of background plasma.

A first difference from the *Lie-Svendsen et al.* [1997] model is our use of two typical shapes of the electron velocity distribution functions, measured at 1 AU by the 3DP instrument on Wind [*Lin et al.*, 1995], as boundary conditions. In the Lie-Svendsen model, the boundary conditions are given deep into the corona where no detailed observations of the VDF are available. The VDF is assumed to be a displaced Maxwellian; but it should be emphasized that this is only a "generally accepted hypothesis," which is not based on any definite observational evidence.

The second difference from the *Lie-Svendsen et al.* [1997] is that we do not use a classical fluid model in order to simulate the solar wind background density. Instead, we choose to use a collisionless background plasma whose VDF is the generalized Lorentzian function described in detail in the exospheric model of *Pierrard and Lemaire* [1996] and applied to the solar wind by *Maksimovic et al.* [1997a] (hereinafter refereed to as MPL). The reason for this choice is that such a purely collisionless approach is as relevant as the classical fluid models in their ability to account for the general properties of the solar wind [*Maksimovic et al.*, 1997a]. Moreover, high-speed and low-speed solar wind background plasma can be simulated with small and large values respectively of the κ parameter.

The paper is organized as follows: In section 2, we describe our model. In the first subsection, the Fokker-Planck equation for the transport of electrons in the solar wind is discussed. We present also the method used to solve this transport equation. In section 2.2, we describe how we compute the characteristics of the background electron population using the MPL model. The third section is devoted to the results of the model in the corona when VDFs measured by Wind are used as boundary conditions at large radial distance. This is an innovative approach, since kinetic models generally consider boundary conditions at the exobase, i.e., at low altitudes in the corona, where the VDF of the particles cannot, in fact, be observed and is usually "guessed." In section 4, we compare our solution with another class of solutions of the Fokker-Planck equation. These other solutions are determined by two boundary conditions (one at low altitude in the collision-dominated region and another at large radial distance in the collisionless region). Finally, in section 5, we discuss the origin of suprathermal tails and the influence of the distribution of the background plasma. Some concluding remarks are also presented in this section.

2. Description of the Model

2.1. Fokker-Planck Equation for Test Electrons

The kinetic transport equation for the evolution of the velocity distribution function $f(\mathbf{r},\mathbf{v},t)$ of the electrons in the solar wind is

$$\frac{\partial f(\mathbf{r},\mathbf{v},t)}{\partial t} + (\mathbf{v}.\nabla_{\mathbf{r}})f(\mathbf{r},\mathbf{v},t) + (\mathbf{a}.\nabla_{\mathbf{v}})f(\mathbf{r},\mathbf{v},t) = \left(\frac{df}{dt}\right)_c \quad (1)$$

where $\mathbf{r}$ and $\mathbf{v}$ are the position and velocity vectors, respectively of the particles; $\mathbf{a}$ is the acceleration due to external forces; and t is the time. In the case of the solar wind, the forces are the electric force, the gravitational force (negligible for the electrons), and the Lorentz force resulting from the magnetic field distribution.

The term on the right-hand side, $(df/dt)_c$, represents the effects of the binary Coulomb collisions. We adopt the Fokker-Planck collision operator appropriate when large-angle deflections can be neglected [*Spitzer*, 1956, *Hinton*, 1983]:

$$\left(\frac{df}{dt}\right)_c = -\frac{\partial}{\partial \mathbf{v}}\left\{\mathbf{A}f(\mathbf{r},\mathbf{v},t) - \frac{1}{2}\frac{\partial}{\partial \mathbf{v}}[\mathbf{D}f(\mathbf{r},\mathbf{v},t)]\right\} \quad (2)$$

where $\mathbf{A}$ is the dynamic friction vector

$$\mathbf{A} = -4\pi\frac{Z_\alpha^2 Z_\beta^2 e^4 \ln\Lambda}{m_\alpha^2}\left(1+\frac{m_\alpha}{m_\beta}\right) \times \int d\mathbf{v}' f_\beta(\mathbf{v}')\frac{(\mathbf{v}-\mathbf{v}')}{(v-v')^3} \quad (3)$$

and $\mathbf{D}$ is the velocity diffusion tensor

$$\mathbf{D} = 4\pi\frac{Z_\alpha^2 Z_\beta^2 e^4 \ln\Lambda}{m_\alpha^2} \times \int d\mathbf{v}' f_\beta(\mathbf{v}')\left[\frac{\mathbf{I}}{v-v'} - \frac{(\mathbf{v}-\mathbf{v}')(\mathbf{v}-\mathbf{v}')}{(v-v')^3}\right]. \quad (4)$$

In (3) and (4), $\ln\Lambda$ is the usual Coulomb logarithm containing the Debye screening effect, $\ln\Lambda \sim 24$. The index α corresponds to the test electrons; β corresponds to the background electrons, m is the mass and Ze is the charge of the particles; $f_\beta(v')$ is the velocity distribution function of the background electrons. Electron-proton collisions are not included here, as in the kinetic solar wind model of *Lie-Svendsen et al.* [1997]. Owing to their small mass ratio, the electron-ion collisions contribute to angular (pitch angle) scattering but not

significantly to the transfer of energy between electrons and protons.

Since in this study we neglect the effects of the angular rotation of the Sun, we assume azimuthal symmetry around the vertical axis, which is then parallel to the magnetic field direction, the gravitational force, and the electric force. A magnetic field distribution $B(r)$ is assumed to be radial, varying as r^{-2} as in most earlier solar wind models such as that of *Lie-Svendsen et al.* [1997]. This assumption is not so unrealistic up to 1 AU. Moreover, it has been shown by *Chen et al.* [1972] that a more realistic spiral magnetic field distribution does not significantly modify the heliocentric distribution of the solar wind density and bulk speed obtained by the exospheric models. We are concerned by stationary solutions of the Fokker-Planck equation. The velocity distribution is then a function of the radial distance r, the velocity v, and $\mu = \cos\theta$, where θ is the angle between the velocity vector and the radial direction. The background electrons are assumed to have a Lorentzian or Kappa velocity distribution function with a nonuniform temperature $T_\beta(r)$, as in the MPL generalized Lorentzian exospheric solar wind model.

Dimensionless velocities are defined by

$$y = \sqrt{\frac{m_\alpha}{2kT_\alpha}}v = \frac{v}{w_\alpha}, \tag{5}$$

$$x = \sqrt{\frac{m_\beta}{2kT_\beta(r)}}v = \frac{v}{w_\beta(r)}. \tag{6}$$

The VDF of the background electrons is assumed to be a nondisplaced Lorentzian (or Kappa) distribution, defined by

$$f_\beta^\kappa(\mathbf{r},\mathbf{v}) = \frac{n_{0\beta}}{2\pi(\kappa w_\beta^2)^{3/2}}\frac{\Gamma(\kappa+1)}{\Gamma(\kappa-1/2)\Gamma(3/2)} \cdot\left(1+\frac{v^2}{\kappa w_\beta^2}\right)^{-(\kappa+1)} \tag{7}$$

where $\Gamma(x)$ is the gamma function, w_β is the thermal speed, m_β is the mass of the particles, $n_{0\beta}$ is the number density at a reference level r_0, and κ is a real number that must be greater than 3/2. With these definitions and assumptions, the Fokker-Planck equation (1) becomes:

$$\begin{aligned}&\frac{\partial f}{\partial t} + w_\beta x\mu\frac{\partial f}{\partial r} + \frac{a(r)}{w_\beta}\left[\mu\frac{\partial f}{\partial x} + \frac{(1-\mu^2)}{x}\frac{\partial f}{\partial \mu}\right] + w_\beta\frac{x}{r}(1-\mu^2)\frac{\partial f}{\partial \mu}\\ &= \sum_\beta 2\pi\frac{Z_\alpha^2 Z_\beta^2 e^4\ln\Lambda}{m_\alpha^2}\left(\frac{m_\beta}{2kT_\beta}\right)^{3/2} n_\beta(r)\times\\ &\left(\frac{\kappa}{(\kappa-3/2)}\frac{[1-\beta_4(b_2)]}{x^2}\times\right.\\ &\left\{\frac{1}{x}\frac{\partial^2 f}{\partial x^2} + \frac{1}{x^2}\left[2\frac{m_\alpha}{m_\beta}\frac{(\kappa-3/2)}{\kappa}x^2 - 1\right]\frac{\partial f}{\partial x}\right\}\\ &+\frac{2A_\kappa}{3\kappa^{3/2}}\left(1+\frac{x^2}{\kappa}\right)^{-\kappa}\times\\ &\left[\frac{\partial^2 f}{\partial x^2} + \frac{2}{x}\left(1+\frac{m_\alpha}{m_\beta}x^2\right)\frac{\partial f}{\partial x} + 6\frac{m_\alpha}{m_\beta}f\right]\\ &\left.+\frac{1}{x^3}\frac{\partial g}{\partial x}\frac{\partial}{\partial \mu}(1-\mu^2)\frac{\partial f}{\partial \mu}\right).\end{aligned} \tag{8}$$

The appendix outlines how this equation has been obtained. The density n_β and the temperature T_β of the background distribution vary with the radial distance.

When the parameter κ tends to the infinity, the right-hand side of (2) tends to the well-known expression of the collision term for a Maxwellian background distribution [*Hinton*, 1983]:

$$\begin{aligned}\left(\frac{df}{dt}\right)_c &= \frac{c_0}{m_\alpha^2}n_\beta(r)\left(\frac{m_\beta}{2kT_\beta}\right)^{3/2}\\ &\times\left\{\frac{1}{x^2}\frac{\partial}{\partial x}\left[\left(2xf\frac{m_\alpha}{m_\beta}+\frac{\partial f}{\partial x}\right)\mathcal{F}(x)\right] + \frac{1}{x^3}\frac{\partial g}{\partial x}\frac{\partial}{\partial \mu}(1-\mu^2)\frac{\partial f}{\partial \mu}\right\}.\end{aligned} \tag{9}$$

This expression for the collision term has been used in the model of *Lie-Svendsen et al.* [1997].

It is convenient to introduce the function $f'(x) = f(x)\exp(x^2)$ and solve (9) and (8) for the f' function. To obtain steady state solutions for the test electron velocity distribution function, we use a specialized spectral method similar to that described by *Pierrard and Lemaire* [1998] for the resolution of the Fokker-Planck equation in the polar wind.

The solution is expanded in terms of Legendre polynomials with respect to $\mu = \cos\theta$ [*Canuto et al.*, 1988]:

$$f(r,x,\mu) = \exp(-x^2)\sum_{l=0}^{n-1} a_l(r,x)P_l(\mu). \tag{10}$$

The coefficients $a_l(r,x)$ in (10) are expanded as a linear combination of N "speed polynomials" $S_s(x)$:

$$f(r,x,\mu) = \exp(-x^2)\left[\sum_{l=0}^{n-1}\sum_{s=0}^{N-1} a'_{ls}(r)P_l(\mu)S_s(x)\right]. \tag{11}$$

The orthogonal speed polynomials have been introduced by *Shizgal and Blackmore* [1984].

The $a'_{ls}(r)$ coefficients are developed in terms of Legendre polynomials for the interval $[0,c]$ with respect to the dimensionless altitude variable, which corresponds to the number of mean free paths, $z = \int_{r_0}^R \sigma(r)n_\beta(r)dr$, where $\sigma(r) = c_0/[2kT_\beta(r)]$. As a result of these polynomial expansions, the VDF is approximated by

$$f(z,x,\mu) = \exp(-x^2) \times \left[\sum_{l=0}^{n-1}\sum_{s=0}^{N-1}\sum_{m=0}^{M-1} a''_{lsm} P_l(\mu) S_s(x) L_m(z)\right]. \quad (12)$$

where n, N, and M are integers whose values are adjusted to obtain the required numerical precision for the solution.

The advantage of this method is that in a discrete ordinate basis, the derivatives of any continuous function $f(y)$ can be approximated by the following expansion:

$$\left(\frac{\partial f}{\partial y}\right)_{y=y_i} \simeq \sum_{j=0}^{N-1} D_{ij} f(y_j) \quad (13)$$

where D_{ij} are the matrix elements of the derivative operator in the polynomial basis [*Shizgal and Blackmore*, 1984]. The coefficients a''_{lsm} of the expansion (13) have to satisfy specific conditions [*Pierrard and Lemaire*, 1998] for the mathematical solutions of the Fokker-Planck equation to be definite positive and not singular for all quadrature points in the configuration space.

The velocity distribution function $f(z,x,\mu)$ is determined at 1 AU from Wind measurements, which are taken as boundary conditions and thus determine the value of the coefficients a''_{lsm} at this refence level. The problem of finding $f(z,x,\mu)$ at the other altitudes is then reduced to a numerical problem of the large matrix inversion:

$$Aa'' = b. \quad (14)$$

For $n = 10$, $N = 10$, and $M = 10$, the matrix A has 1000×1000 elements and the matrices a'' and b have 1000×1 elements. We have checked that a minimum of six polynomials of each variable x, μ, and z is required to obtain results that do not change significantly when n, N, or M is increased by one unit. In all practical cases, we choose 10 polynomials for each variable so that the results have a precision better than 10% with reasonably short CPU times. We obtain then 1000 values of a''_{lsm} which are solutions of the Fokker-Planck equation at 10 different altitudes between 1 AU and 4 R_s. We use several successive steps in radial distance in order to have a finer scale in the corona, where the density gradient is larger than at large distances.

2.2. The Exospheric Background Electrons

Density, temperature, and electric potential profiles of the background electrons are taken from the Lorentzian exospheric model (MPL) [*Pierrard and Lemaire*, 1996; *Maksimovic et al.*, 1997a]. In this exospheric model, the plasma is considered to be collisionless above a level situated at a radial distance between 3 and 10 R_s in the solar wind and called the exobase [*Lemaire and Scherer*, 1971a, b]. It means that in the exosphere, the collision term $(df/dt)_c$ is neglected in (8), which then becomes the Vlasov equation.

In the exospheric approach of the problem, the solar wind is accelerated by the ambipolar electrostatic potential. This potential is needed to provide the equality of the proton and electron fluxes. *Maksimovic et al.* [1997a] have shown that when the electron suprathermal tails are enhanced at the exobase, the ambipolar electric potential is increased and the electrons can reach higher bulk velocities, up to 600 km/s at 1 AU. Elsewhere, this result is somehow supported by *Maksimovic et al.* [1997b]. These authors fitted ≈16,000 Ulysses electron VDFs with Kappa functions and showed a clear correlation between the solar wind bulk speed and the strength of suprathermal tails in the electron VDFs. Moreover, the Lorentzian exospheric solar wind model is supported by the fact that the electron VDFs, obtained in the low corona, exhibit suprathermal tails (see next section).

Since we study in section 3 the radial evolutions of two typical electron VDFs observed at 1 AU, one for the slow solar wind and one for the high-speed streams, we will consider two different backgrounds. For the low-speed solar wind, the background is obtained by computing the MPL model from an exobase located at $r_0 = 5.6 R_s$ and with the following conditions: $\kappa_p = \infty$, $\kappa_e = \infty$ (i.e., Maxwellian background plasma), $n_e(r_0) = n_p(r_0) = 5.2 \times 10^{10}$ m^{-3}, $T_p(r_0) = 10^6$ K, $T_e(r_0) = 1.5 \times 10^6$ K. Under these exobase conditions, the solar wind velocity is 300 km/s at 1 AU. For the high-speed solar wind background, the same conditions are assumed at the exobase except that $\kappa_e = 3$, so that the background high-velocity plasma reaches then an expansion velocity of 500 km/s at 1 AU.

Note that these densities and temperatures are chosen so that the background electrons and protons both become "collisionless" at the same exobase altitude, i.e., at 5.6 R_s (see MPL for more details). The background density, temperature, bulk velocity, and electric potential profiles are plotted in Figure 1 for both cases.

In our model, as in the work by *Lie-Svendsen et al.* [1997], the dynamic friction vector **A** and the velocity diffusion tensor **D** are evaluated under the assumption that the velocity distribution of the target background particles does not have a bulk velocity. This is, of course, a questionable assumption in these models, since the background electrons of the actual solar wind do have an expansion velocity. One can argue, however, that the thermal speed of the background electrons (>1,500 km/s) is larger than their radial bulk speed (<600 km/s). Therefore the small asymmetry introduced by a non zero bulk speed is of little importance. Furthermore, solar wind ions are accelerated by the electric potential created by the escaping electrons of the tails of the VDF as described in the Lorentzian model [*Maksimovic et al.*, 1997a].

More essentially, we wish to determine how the tails of the solar wind electron VDF change as a function

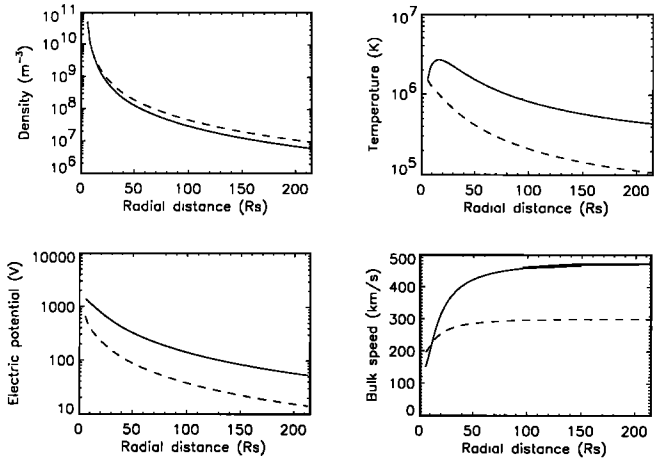

Figure 1. The radial distribution of the background density, temperature, electric potential and bulk velocity determined by the exospheric kappa model with $\kappa = \infty$ (dashed line) for the electrons in the low-speed solar wind and with $\kappa = 3$ (solid line) in the high-speed solar wind.

of the heliocentric distance. Given the observed distribution at 1 AU, we infer the magnitude of the electron VDF suprathermal tails at 4-5 R_s, the electron escape flux, and the value of the thermoelectric potential that is associated with it. Note also that assuming a nondisplaced Maxwellian or a Kappa VDF for the target background electrons is reasonable, since all electrons that have energies smaller than the electrostatic potential barrier are unable to escape and do not contribute to the net escape flux of the electrons. Therefore their velocity distribution should be symmetric in the vertical direction, unlike the displaced VDF with a nonzero bulk speed used in hydrodynamical models. As a consequence, assuming a static electron background is more realistic than one may consider at first glance, as a result of the paradigm imposed for more than three decades by hydrodynamical and MHD models of the solar wind.

3. Results of the Model: Radial Evolution of Test Electron VDFs

Typical electron velocity distribution functions measured by the electrostatic analyzer of the 3DP instrument on Wind [*Lin et al.*, 1995] at 1 AU are illustrated in Figure 2. These distributions are corrected for the spacecraft potential and are given in the solar wind bulk frame of reference, which in our static background model is assumed to have a zero bulk speed. The first VDF (case a) is obtained in a typical slow speed solar wind ($v = 320$ km/s, $n_e = 10$ cm^{-3}). The distribution has a nearly isotropic and Maxwellian thermal core and a hot halo population whose energy spectrum decreases as a power law with the energy (see Figure 2a). The second distribution (case b) is more typical of the high-speed solar wind ($v = 650$ km/s, $n_e = 4$ cm^{-3}). The electron velocity distribution function is more anisotropic and contains a population of strahl electrons aligned with the local magnetic field direction, as illustrated in Figure 2b. When fitting these two distributions with Lorentzian or Kappa functions, we find $\kappa \simeq 3.1$ for case a and $\kappa \simeq 2$ for case b.

No solar wind observations are available closer to the Sun than 0.3 AU [*Pilipp et al.*, 1987]. At this radial distance, the Coulomb collisions are more important. By solving the Fokker-Planck equation, we determine the electron velocity distribution function at 4 R_s in the corona using the observed velocity distribution functions at 215 R_s (1 AU) as boundary conditions.

Figures 3a and 3b illustrate the calculated velocity distribution functions obtained at 4 R_s with the model described in the previous sections for low-speed and high-speed, respectively, typical electron VDFs. It can be seen that the importance of the core electrons increases in the corona, owing to the increasing importance of Coulomb collisions, which tend to produce an isotropic and Maxwellian VDF for the test electrons that is close to the isotropic and Maxwellian distribution of the background electrons. The Coulomb collisions have larger effects on the low-energy particles than on the suprathermal halo electrons. Electrons of higher energy are less affected by the Coulomb collisions, since their cross section varies as v^4. As a con-

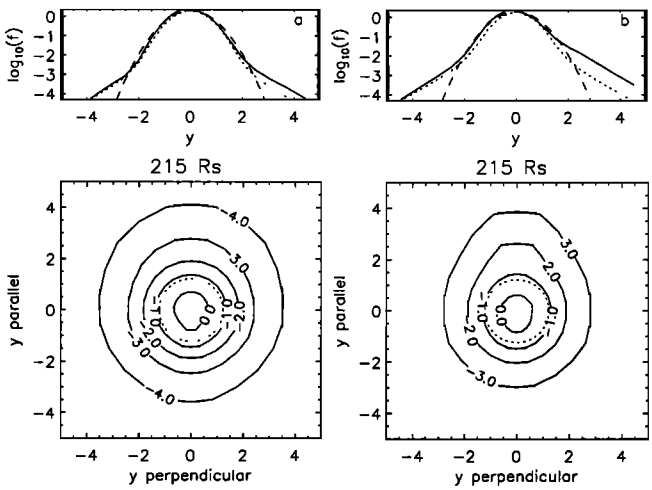

Figure 2. Typical electron velocity distribution functions measured by the electrostatic analyzer 3DP on Wind and taken as a boundary condition at 1 AU, typical of the (a) low-speed solar wind, measured on January 24, 1997, at 1834 UT, and (b) high-speed solar wind, measured on the January 28, 1997 at 1336 UT. Cross sections of the phase space density are plotted as a function of the normalized velocity parallel $y_\parallel$ (solid lines) and perpendicular $y_\perp$ (dotted lines) to the magnetic field direction. The Maxwellian velocity distribution with the same thermal speed is shown by a dashed line. (bottom) Velocity distribution functions represented by isocontours of constant phase space density in the $y_\parallel, y_\perp$ plane. The dotted circle corresponds to the Maxwellian thermal velocity $y = \sqrt{3/2}$.

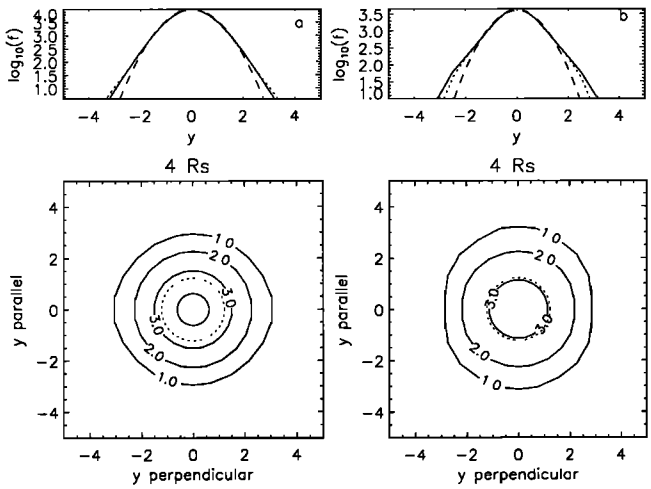

Figure 3. Same as Figure 2, but for electron velocity distribution functions obtained at 4 R_s by solving the Fokker-Planck equation with the velocity distribution functions presented in Figure 2 taken as a boundary condition at 1 AU, for the (a) low-speed and (b) high-speed solar wind. Note that the phase space density is 4 orders of magnitude larger at 4 R_s in the corona than in Figure 2, at 1 AU.

sequence, the non-Maxwellian "halo" population is already present in the VDF at low altitudes. This implies that the suprathermal electrons observed at large distances in the solar wind have their origin in the inner corona: halo electrons are already created deep into the solar corona by a process not yet clearly identified.

For the low-speed solar wind case illustrated in Figures 2a and 3a, the VDF of the test electrons is close to a Maxwellian distribution at 4 R_s. Nevertheless, a suprathermal tail is still present. This distribution at 4 R_s can be fitted with a Lorentzian function with a Kappa index equal to $\kappa \sim 10$.

In the high-speed solar wind, the VDF has a more important tail at 1 AU. Moreover, we assume here that the background electrons have a Lorentzian distribution with important suprathermal tails ($\kappa_e = 3$). The VDF found at 4 R_s has then a more enhanced suprathermal tail than in the case of the low-speed solar wind. A fit of this VDF with a Lorentzian distribution gives $\kappa \sim 4$, which is not too far from the suprathermal strength of the background electron distribution ($\kappa_e = 3$). Note that this latter result is basically unchanged if we use a Maxwellian background instead of a Lorentzian one. Even if the VDF's suprathermal tails at 4 R_s have their strength attenuated with the use of a Maxwellian background, they are still present in the corona.

It is well known that the density in coronal holes, which are the source of the fast wind, is lower than in the other regions of the solar corona. When the density of the background electrons in the coronal holes is reduced, the tail in the VDF found at 4 R_s becomes more prominent, since then the Coulomb collisions are less efficient to transfer momentum and energy to the test particles.

The anisotropy of the VDF exists at all radial distances, from 4 R_s to 1 AU; although the anisotropy is relatively small at 4 R_s, owing to the large values of the core and halo VDF at this altitude. A small anisotropy is thus sufficient to create the important "strahl" component observed at large radial distances in the solar wind.

As pointed out by *Lie-Svendsen et al.* [1997], no self-consistent study of the radial distribution of the electron VDFs has yet been carried out. The background or target electrons differ from the test electrons. In order to remediate partially this limitation and to simulate "self-collisions," we have applied the following procedure. The moments of the test electrons are calculated from the velocity distribution function found by solving the Fokker-Planck equation. The density is given by

$$n(r) = \int f(r, v, \mu)\, d\mathbf{v}. \tag{15}$$

The temperature corresponds to a second-order moment of the velocity distribution:

$$T(r) = \frac{1}{3}\left[T_{\|}(r) + 2T_{\perp}(r)\right] \tag{16}$$

where

$$T_{\|}(r) = \frac{m \int v_{\|}^2 f(r, v, \mu)\, d\mathbf{v}}{kn(r)} \tag{17}$$

$$T_{\perp}(r) = \frac{m \int v_{\perp}^2 f(r, v, \mu)\, d\mathbf{v}}{2kn(r)}. \tag{18}$$

The integrals on the right-hand side of (15), (17), and (18) are easily performed by numerical quadrature taking into account the polynomial expansion (13) of the VDF [see *Pierrard*, 1997].

We then use the density and temperature calculated for the test electrons for a second step iteration. We recompute the solution of the Fokker-Planck equation to determine a second approximation of the VDF of the test electrons. We continue this process until the difference between successive iterations is smaller than 5% for all energies. The convergence is very fast; indeed, the calculated density and temperature profiles for the test electrons are not very different from the ones of the background distribution.

This procedure allows us to simulate iteratively self-collisions, although the expressions of the diffusion coefficient **D** and friction tensor **A** are based on the assumption that the velocity distribution function of the background particles is fully Lorentzian and isotropic. Figure 3 shows, however, that this is not exactly the case, since the actual VDF is asymetric and not precisely Lorentzian.

4. Model With Boundary Conditions at Two Different Altitudes

The solution of the Fokker-Planck equation depends on the boundary conditions. The choice of the boundary conditions is generally assumed depending on the expected collisional state of the plasma at a reference altitude.

Collisional models of polar and solar wind with two boundary conditions, one at low altitude and one at high altitude, have been developed by *Barghouthi et al.* [1993], *Lie-Svendsen and Rees* [1996], and *Lie-Svendsen et al.* [1997]. These models are used, like ours, to determine the velocity distribution function of the particles in the transition region between the collision-dominated plasma and the collisionless plasma at large radial distances. They are based on particle-in-cell simulations or on the resolution of the Fokker-Planck equation by a finite difference numerical scheme. Such models have been applied to the study of the distribution of hydrogen and helium ions in the terrestrial polar wind. In all these models, the boundary conditions are assumed both at low altitude and high altitude.

At low altitude, the outward moving particles are assumed to be distributed according to an isotropic and Maxwellian VDF:

$$f(y, r_0, \mu > 0) = n_0 \left(\frac{m}{2kT\pi}\right)^{3/2} \exp(-y^2) \qquad (19)$$

At high altitude, the VDF is assumed to be truncated as in exospheric models: there are no particles coming from the interplanetary space in the downward loss cone, except trapped and ballistic particles that have been reflected at higher altitudes because they had not enough energy to escape:

$$f(y > y_{esc}, r_1, \mu < 0) = 0 \qquad (20)$$

$$f(y < y_{esc}, r_1, \mu < 0) = f(y < y_{esc}, r_1, \mu > 0) \qquad (21)$$

This choice of boundary conditions is a standard one and has been justified theoretically by arguing that collisions at low altitude maintain a nearly isotropic and Maxwellian VDF, while at high altitude, the particles with energies high enough to escape never return back. However, these boundary conditions are ad hoc, as in earlier exospheric models. Furthermore, the observations show that the VDF at any radial distance has not necessarily a Maxwellian (exponential) tail, but usually an enhanced population of suprathermal particles whose energy spectrum is better fitted by a power law instead of an exponential. In addition, any observed VDF is generally not so sharply truncated as imposed by (20) and (21), nor at high altitudes, nor a fortiori at the exobase. At low altitudes, only the upward part of the distribution is assumed to be Maxwellian. This ad hoc assumption is reminiscent of the hypothesis on which the early exospheric models of *Jeans* [1923] had been based and was popularized by *Lemaire and Scherer* [1970] in their exospheric or zero-order kinetic model of the polar wind. It should be emphasized that such assumptions were taken as a simple first-order approximation and postulated for convenience. Indeed, they allow the derivation of simple analytic expressions of the moments of the VDF, but such ad hoc boundary conditions are not absolute needs. However, discontinuities of zero and first order are artificial, and they are not expected to exist in actual velocity distribution functions observed in the polar and solar wind. The VDF has to be somehow asymmetric to provide the upward flux of particles and energy. In fact, the actual VDF at low altitude is unknown a priori but has to be calculated a posteriori by solving the FPE. It is this alternative reasoning that led us to fix the boundary conditions at 1 AU from Wind observations in order to determine the shape of the electron distributions lower in the corona. Therefore it is interesting to compare the results of our collisional model using similar boundary conditions, not only at high altitudes but also at low altitudes, deep in the collision-dominated region where a Maxwellian VDF is a generally accepted approximation for upward moving particles.

The VDFs for such an alternative kinetic model of the solar wind electrons are presented on Figure 4. At high altitudes, the results of our alternative model are near to truncated Maxwellians obtained at the exobase in the exospheric models of *Lemaire and Scherer* [1970]. This happens to be the case since we impose quite similar conditions at the top of the simulation region, as those imposed at the exobase in their collisionless models. Furthermore, we impose a Maxwellian distribution

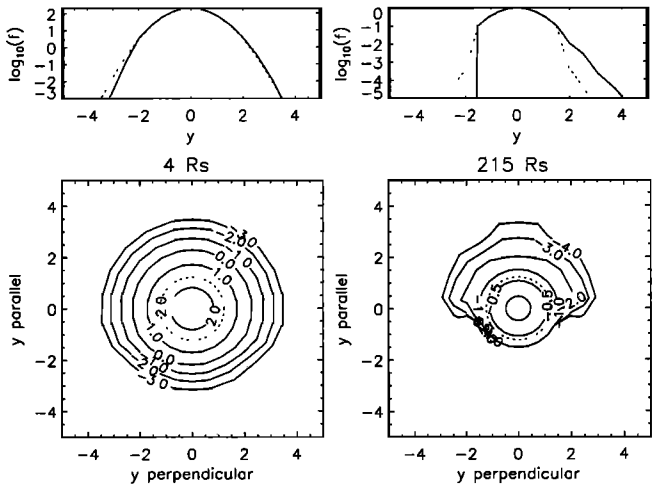

Figure 4. Velocity distribution function (VDF) of electrons at (left) 215 and (right) 4 R_s in a collisional model with two boundary conditions, one at high altitude where the VDF is void of particles coming in from infinity and one at low altitude where an isotropic and Maxwellian VDF is assumed for upward moving particles. At low altitude (4 R_s), the electrons moving upward are assumed to have a Maxwellian VDF with a temperature $T = 1.5 \times 10^6$ K as in the model of *Lie-Svendsen et al.* [1997].

as a boundary condition at low altitudes. Indeed, a Maxwellian is an obvious solution of the Fokker-Planck equation. Note that unlike in the calculations of *Lie-Svendsen et al.* [1997], our solutions of the FP equation do not show a well-focused, beam-like feature at high energies for $\mu = 1$. However, as in the *Lie-Svendsen et al.* [1997] calculations, imposing a Maxwellian VDF at the base of our two boundaries model does not produce the suprathermal halo component that is observed at 1 AU.

In our alternative solution of the FP equation, the angular distribution is truncated at the high-altitude boundary: $f(v_{\|}, v_{\perp})$ has a zero-order discontinuity at $v_{\|} = 0$ (i.e., $\mu = 0$) that is similar to that of exospheric model at the exobase. The origin of this discontinuity is a consequence of this special choice of boundary conditions.

The radial distribution of the electron density and temperature in this "two boundary condition model" are illustrated on Figure 5 by dashed lines. Solid lines show the distribution assumed for the background electrons, while the dashed lines correspond to those of the test electrons after a few successive iterations. It can be seen that the radial density (i.e., the zero-order moment of the VDF) is not very sensitive to the type of model (kinetic, exospheric, hydrodynamic) adopted. Therefore it would be difficult to favor one type of model description over the others, just on the basis of observed density or even of the average temperature distribution as a function of heliocentric distance. However, the bulk velocity and the higher odd moments of the VDF are much more sensitive to the anisotropy of the VDF and its energy spectra.

5. Summary and Discussion

Solar wind electron VDFs observed in the inner heliosphere exhibit a large suprathermal halo component, whose origin is still not understood. Does this halo population have a coronal origin, or is it a by-product of some sophisticated wave-particle interaction or other ad hoc process? The aim of this paper is to determine whether electron VDFs with suprathermal tails already exist in the low corona and how prominent these tails are there.

In order to answer to this question, we have solved the Fokker-Planck equation for test electrons that are scattered by a given background solar wind plasma. As test particles, we use velocity distribution functions observed at 1 AU by the 3DP instrument on board the Wind spacecraft. This is our upper boundary condition. The density and temperature distributions obtained with the Lorentzian exospheric solar wind model [*Maksimovic et al.*, 1997a] have been used to simulate the corresponding distributions of the background or target particles.

Our results indicate that suprathermal tails must exist in the lower corona when they are observed at 1 AU; but they are much less important close to the Sun than those measured at larger distances. We have examined two different cases: (1) case a, a typical low-speed solar wind with a Maxwellian background plasma ($\kappa_e = \infty$), where at 1 AU, the VDF of the test electrons is fitted with a Lorentzian function corresponding to $\kappa = 3.6$; and (2) case b, a typical high-speed solar wind with a Lorentzian background plasma with suprathermal particles ($\kappa_e = 3$), where at 1 AU, the VDF of the test electrons is fitted by a Lorentzian whose index kappa is equal to $\kappa = 2.4$. Integrating the Fokker-Planck equation for the test electrons from 1 AU to 4 R_s, we find that the electron VDFs have less important suprathermal tails in the low corona, corresponding to $\kappa = 10.1$ for the slow wind model (case a) and to $\kappa = 4.2$ for the fast wind model (case b). As expected, the suprathermal tails are less attenuated by Coulomb collisions in the fast wind than in the slow one.

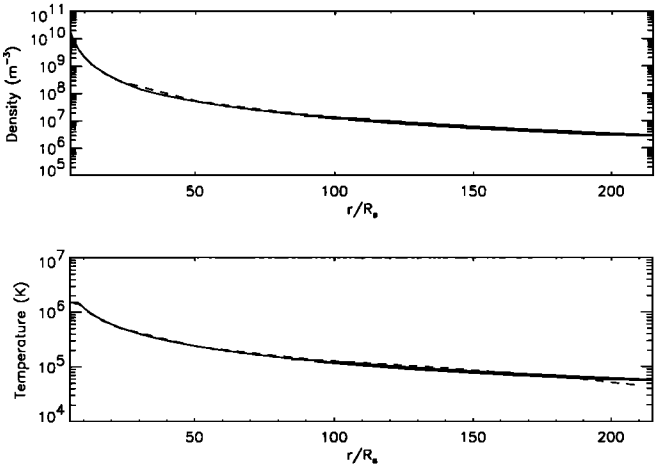

Figure 5. (top) Density and (bottom) temperature as a function of the radial distance in solar radius for the two boundary condition model. The solid line corresponds to the background model, and the dashed line corresponds to the test electron model.

5.1. On the Choice of Background VDF

How important is the velocity distribution function of the background electrons in our modelization? To investigate this point, we have run our model, for the high speed solar wind case, with a Maxwellian background. The result is that, in such a configuration, the test particles VDF obtained at 4 R_s can be fitted by a generalized Lorentzian function whose index kappa is equal to $\kappa = 6.5$. Therefore it appears that a Maxwellian background does not completely remove suprathermal tails from the VDF deep in the corona. The suprathermal tails obtained at 4 R_s in Figure 3b are not only due to the assumption that the background plasma has an enhanced suprathermal tail but are essentially the consequence of electron velocity distribution functions decreasing as a power law of the energy at large radial distances. However, this result shows that in this type of collisional kinetic model, the shape

of the background particles plays a nonnegligible role. This is why we have included the halo electrons in our background by using a Lorentzian background. Finally, note that, as mentioned previously, all our results are obtained under a set of specific assumptions that may not all be satisfied in interplanetary space. In particular, we have neglected electron-ion collisions as well as wave-particle interactions, which can contribute also to some extent to pitch angle scattering. Examining the effects of electron-ion collisions on our present conclusions constitutes a future study.

5.2. Comparisons With Previous Models and Observations

To some extent, the present results support the Lorentzian exospheric model [*Pierrard and Lemaire*, 1996; *Maksimovic et al.*, 1997a], which demonstrates that electron VDFs with large suprathermal tails could increase the electric potential required to provide the equality of the electrical currents and then accelerate the solar wind protons and other positive ions to higher bulk speed.

From the present study, it appears that starting with Maxwellian distributions in the corona, there is no way to produce suprathermal tails in the solar wind if external forces and Coulomb collisions are the only processes acting in the solar wind. The Maxwell-Boltzman function is an exact solution of the Fokker-Planck equation, but it corresponds to a corona in hydrostatic equilibrium.

Generally speaking, the pioneer work of *Scudder* [1992 a, b] and the results presented here provide an alternative point of view for solar wind acceleration. Unlike in hydrodynamic solar wind models, there is no need to invoke ad hoc momentum transfer or energy deposition in the corona, nor MHD waves, to reach high bulk velocity in the solar wind. The high speed solar wind can be considered to be the result of large suprathermal tails, which are effectively observed in the solar wind at 1 AU [*Maksimovic et al.*, 1997b] and should exist at low altitude in the corona. The low-speed solar wind is characterized by VDF with reduced suprathermal tails. The moment description of the solar wind expansion by *Leblanc and Hubert* [1997] emphasizes also the importance of high-energy tails in the acceleration process of the particles.

Note that our results agree also with the study by *Ko et al.* [1996]. These authors have inferred electron VDFs in the lower solar corona from measurements of the charge states of solar wind ions at 1 AU. They have shown that electron VDF with suprathermal tails corresponding to Lorentzian VDFs with κ ranging from 5 to 10 have to be assumed in the lower corona in order to account for the charge state of ions observed at 1 AU. With our model, we have obtained, at 4 R_s, a VDF that is well fitted by a $\kappa = 10$ Lorentzian function in the case of a Maxwellian background corresponding to the low-speed solar wind; a $\kappa = 4.2$ Lorentzian fits the electron VDF at 4 R_s in the case of the high-speed solar wind with a $\kappa = 3$ Lorentzian background.

The present study indicates that exospheric models of the solar wind, like the generalized Lorentzian model or Kappa model (which includes the early Maxwellian exospheric model as a limiting case for $\kappa \to \infty$), are rather useful zero-order kinetic models of the solar coronal evaporation. Indeed, a great advantage of these models is that they are analytic and have been able to outline the physical origin of the thermoelectrostatic field accelerating the coronal ions to supersonic solar wind velocities. Moreover, these exospheric models provide realistic approximate density and temperature distributions in the solar wind. They have also proven to be valuable for studying the asymptotic behavior of the moment profiles at large heliocentric distances [*Meyer-Vernet and Issautier*, 1998]. Of course, the artificial discontinuity inherent in exospheric VDFs does not exist in the actual velocity distribution functions observed in the solar wind. The sharp exobase level is a mathematical simplification that has been overcome in this paper, where a post exospheric model of the solar wind electrons is proposed. A new step has been bridged that has freed the solution of the FP equation from such ad hoc and somewhat artificial assumptions about the VDF at the upper and lower boundaries. The VDFs imposed at 1 AU, which were determined from Wind observations, have no discontinuities in velocity that exist in simple exospheric models.

Appendix

A1. Diffusion and Friction Coefficients for a Lorentzian Function

The Coulomb collision term can be written [*Hinton*, 1983]:

$$\left(\frac{df}{dt}\right)_c = \sum_\beta 4\pi \frac{Z_\alpha^2 Z_\beta^2 e^4 \ln\Lambda}{m_\alpha^2} \cdot\left[-\left(1+\frac{m_\alpha}{m_\beta}\right)\frac{\partial}{\partial v_i}\left(f\frac{\partial h_\beta}{\partial v_i}\right) + \frac{1}{2}\frac{\partial^2}{\partial v_i \partial v_j}\left(f\frac{\partial^2 g_\beta}{\partial v_i \partial v_j}\right)\right] \quad \text{(A1)}$$

where the functions $h_\beta(\mathbf{r},\mathbf{v})$ et $g_\beta(\mathbf{r},\mathbf{v})$ are defined by

$$h_\beta = \int \frac{f_\beta(\mathbf{r},\mathbf{v}')}{|\mathbf{v}-\mathbf{v}'|}d\mathbf{v}' \quad \text{(A2)}$$

$$g_\beta = \int f_\beta(\mathbf{r},\mathbf{v}')|\mathbf{v}-\mathbf{v}'|d\mathbf{v}'. \quad \text{(A3)}$$

Here $f_\beta(\mathbf{r},\mathbf{v}')$ are the velocity distribution functions of the background or target particles β with which the test particles α collide. In the following, we will use the normalized velocity variables x and y:

$$x = \sqrt{\frac{m_\beta}{(2kT_\beta)}}v = y\frac{w_\alpha}{w_\beta}. \quad \text{(A4)}$$

A1.1. Maxwellian Distribution. The integrals (A2) and (A3) have been calculated analytically. For an isotropic Maxwellian distribution, *Lie-Svendsen* [1996] and *Pierrard and Lemaire* [1998] find that (A1) can be written:

$$\left(\frac{df}{dt}\right)_c = 2\pi\frac{Z_\alpha^2 Z_\beta^2 e^4 \ln\Lambda}{m_\alpha^2}\left(\frac{m_\beta}{2kT_\beta}\right)^{3/2} n_\beta \exp(-q_\beta(r)) \cdot\left[\frac{\partial^2}{\partial\mathbf{x}\partial\mathbf{x}} : \left(f\frac{\partial^2 g}{\partial\mathbf{x}\partial\mathbf{x}}\right) -2\left(1+\frac{m_\alpha}{m_\beta}\right)\frac{\partial}{\partial\mathbf{x}}\cdot\left(f\frac{\partial h}{\partial\mathbf{x}}\right)\right] \quad \text{(A5)}$$

where

$$h(x) = \int \frac{1}{\pi^{3/2}}\frac{\exp(-x'^2)}{|\mathbf{x}-\mathbf{x}'|}d\mathbf{x}' = \frac{\mathrm{erf}(x)}{x} \quad \text{(A6)}$$

$$g(x) = \int \frac{1}{\pi^{3/2}}\exp(-x'^2)|\mathbf{x}-\mathbf{x}'|d\mathbf{x}' = \mathrm{erf}(x)\left(x+\frac{1}{2x}\right)+\frac{1}{\sqrt{\pi}}\exp(-x^2) \quad \text{(A7)}$$

where $\mathrm{erf}(x)$ is the "error" function:

$$\mathrm{erf}(x) = \frac{2}{\sqrt{\pi}}\int_0^x \exp(-\xi^2)d\xi \quad \text{(A8)}$$

Since the background velocity distribution function is assumed to be isotropic, the anisotropies and asymmetries of the calculated test particles VDF can only be attributed to the boundary conditions.

A1.2. Lorentzian Distribution. Analytic expressions for the integrals (A6) and (A7) can also be obtained for other VDFs and, in particular, for an isotropic generalized Lorentzian or Kappa function:

$$f_\beta^\kappa(\mathbf{x}') = \frac{n_{0\beta}}{2\pi(\kappa w_\beta^2)^{3/2}}A_\kappa\left(1+\frac{x'^2}{\kappa}\right)^{-(\kappa+1)}, \quad \text{(A9)}$$

where

$$x' = \sqrt{\frac{m_\beta}{2kT_\beta}}v' = \frac{v'}{w_\beta} \quad \text{(A10)}$$

$$A_\kappa = \frac{\Gamma(\kappa+1)}{\Gamma(\kappa-1/2)\Gamma(3/2)}. \quad \text{(A11)}$$

The diffusion coefficient $\mathbf{D}$ is given by

$$\mathbf{D} = 2\frac{c_0}{m_\alpha^2}\frac{2kT_\beta}{m_\beta}\frac{\partial^2}{\partial\mathbf{x}\partial\mathbf{x}}\int d\mathbf{x}' f_\beta(x')|\mathbf{x}-\mathbf{x}'|. \quad \text{(A12)}$$

In polar coordinates (x', μ, ϕ), this integral is:

$$\mathbf{D} = 4\pi\frac{c_0}{m_\alpha^2}\frac{2kT_\beta}{m_\beta}\frac{\partial^2}{\partial\mathbf{x}\partial\mathbf{x}}\int_0^\infty dx' x'^2 f_\beta(x') \int_{-1}^1 d\mu\sqrt{x^2+x'^2-2xx'\mu} \quad \text{(A13)}$$

$$\mathbf{D} = 4\pi\frac{c_0}{m_\alpha^2}\frac{2kT_\beta}{m_\beta}\frac{\partial^2}{\partial\mathbf{x}\partial\mathbf{x}}\int_0^\infty dx'\frac{x'^2}{3xx'}f_\beta(x') \left[(x+x')^3-|x-x'|^3\right] \quad \text{(A14)}$$

$$\mathbf{D} = \frac{4\pi}{3}\frac{c_0}{m_\alpha^2}\frac{2kT_\beta}{m_\beta}\frac{\partial^2}{\partial\mathbf{x}\partial\mathbf{x}} \cdot\left[\int_0^x dx'\left(6xx'^2+2\frac{x'^4}{x}\right)f_\beta(x') +\int_x^\infty dx'(6x'^3+2x^2x')f_\beta(x')\right]. \quad \text{(A15)}$$

The friction term $\mathbf{A}$ is given by

$$\mathbf{A} = 2\frac{c_0}{m_\alpha^2}\left(1+\frac{m_\alpha}{m_\beta}\right)\sqrt{\frac{2kT_\beta}{m_\beta}} \cdot\frac{\partial}{\partial\mathbf{x}}\int d\mathbf{x}'\frac{f_\beta(x')}{|\mathbf{x}-\mathbf{x}'|} \quad \text{(A16)}$$

$$\mathbf{A} = 4\pi\frac{c_0}{m_\alpha^2}\left(1+\frac{m_\alpha}{m_\beta}\right)\sqrt{\frac{2kT_\beta}{m_\beta}} \cdot\frac{\partial}{\partial\mathbf{x}}\left[\int_0^x dx' f_\beta(x')\frac{2x'^2}{x} +\int_x^\infty dx' f_\beta(x')2x'\right]. \quad \text{(A17)}$$

For the generalized Lorentzian function defined in (A9), the integrals become

$$\mathbf{A}_\kappa = 2\frac{c_0}{m_\alpha^2}\left(1+\frac{m_\alpha}{m_\beta}\right)\frac{m_\beta}{2kT_\beta}n_\beta\frac{\partial h_\kappa}{\partial\mathbf{x}} \quad \text{(A18)}$$

$$\mathbf{D}_\kappa = 2\frac{c_0}{m_\alpha^2}\sqrt{\frac{m_\beta}{2kT_\beta}}n_\beta\frac{\partial^2 g_\kappa}{\partial\mathbf{x}\partial\mathbf{x}} \quad \text{(A19)}$$

where

$$h_\kappa = \frac{1}{x}[1-\beta_2(b_2)]+\frac{A_\kappa}{\kappa^{3/2}}\left(1+\frac{x^2}{\kappa}\right)^{-\kappa} \quad \text{(A20)}$$

$$g_\kappa = x[1-\beta_2(b_2)]+\frac{\kappa}{3x}\frac{A_\kappa}{A'_\kappa}[1-\beta_4(b_2)] +\frac{A_\kappa}{\kappa^{3/2}}\left(1+\frac{x^2}{\kappa}\right)^{-\kappa} \cdot\left[\frac{\kappa}{\kappa-1}(x^2-1)+\frac{x^2}{3}\right] \quad \text{(A21)}$$

and where

$$\beta_2(b_2) = \int_0^{b_2} A_\kappa t^{\kappa-3/2}(1-t)^{1/2}dt = 1-\int_{b_2}^1 A_\kappa t^{\kappa-3/2}(1-t)^{1/2}dt \quad \text{(A22)}$$

$$\beta_4(b_2) = \int_0^{b_2} A_\kappa t^{\kappa-5/2}(1-t)^{3/2}dt \quad \text{(A23)}$$
$$= 1 - \int_{b_2}^{1} A_\kappa t^{\kappa-5/2}(1-t)^{3/2}dt$$

$$b_2 = \left(1+\frac{x^2}{\kappa}\right)^{-1}. \quad \text{(A24)}$$

A2. Expression of Collision Term for a Lorentzian Distribution

The collision term (A5) can be explicitely expressed in spherical coordinates:

$$\left(\frac{df}{dt}\right)_c = \sum_\beta 2\pi \frac{Z_\alpha^2 Z_\beta^2 e^4 \ln\Lambda}{m_\alpha^2}\left(\frac{m_\beta}{2kT_\beta}\right)^{3/2} n_\beta \cdot\left[\frac{2}{x^2}\frac{\partial g}{\partial x}\frac{\partial f}{\partial x} + \frac{\partial^2 g}{\partial x^2}\frac{\partial^2 f}{\partial x^2} + \frac{1}{x^3}\frac{\partial g}{\partial x}\frac{\partial}{\partial \mu}(1-\mu^2)\frac{\partial f}{\partial \mu} + 2\frac{\partial f}{\partial x}\frac{\partial \Delta g}{\partial x} - 2\left(1+\frac{m_\alpha}{m_\beta}\right)\left(f\Delta h + \frac{\partial h}{\partial x}\frac{\partial f}{\partial x}\right) + f\Delta^2 g\right] \quad \text{(A25)}$$

where Δ is the Laplacian

$$\Delta = \frac{\partial^2}{\partial x^2} + \frac{2}{x}\frac{\partial}{\partial x} + \frac{1}{x^2}\frac{\partial}{\partial \mu}(1-\mu^2)\frac{\partial}{\partial \mu}. \quad \text{(A26)}$$

A2.1. Maxwellian Distribution. Thus for a Maxwellian distribution, the expression of the collision term is given by

$$\left(\frac{df}{dt}\right)_c = \sum_\beta 2\pi \frac{Z_\alpha^2 Z_\beta^2 e^4 \ln\Lambda}{m_\alpha^2}\left(\frac{m_\beta}{2kT_\beta}\right)^{3/2} n_\beta \cdot\left\{\frac{\mathrm{erf}(x)}{x^2}\left[\frac{1}{x}\frac{\partial^2 f}{\partial x^2} + \frac{1}{x^2}\left(2\frac{m_\alpha}{m_\beta}x^2 - 1\right)\frac{\partial f}{\partial x}\right] + 2\frac{\exp(-x^2)}{\pi^{1/2}x^2}\left[-\frac{\partial^2 f}{\partial x^2} + \left(\frac{1}{x} + 2x - 2\frac{m_\alpha}{m_\beta}x\right)\frac{\partial f}{\partial x} + 4\frac{m_\alpha}{m_\beta}x^2 f\right] + \frac{1}{x^3}\frac{\partial g}{\partial x}\frac{\partial}{\partial \mu}(1-\mu^2)\frac{\partial f}{\partial \mu}\right\}. \quad \text{(A27)}$$

Defining the function

$$\mathcal{F}(x) = \frac{\mathrm{erf}(x)}{x} - \frac{2}{\sqrt{\pi}}\exp(-x^2), \quad \text{(A28)}$$

one finds the usual expression:

$$\left(\frac{df}{dt}\right)_c = \frac{c_0}{m_\alpha^2} n_\beta(r)\left(\frac{m_\beta}{2kT_\beta}\right)^{3/2} \times \left\{\frac{1}{x^2}\frac{\partial}{\partial x}\left[\left(2\frac{m_\alpha}{m_\beta}xf + \frac{\partial f}{\partial x}\right)\mathcal{F}(x)\right] + \frac{1}{x^3}\frac{\partial g}{\partial x}\frac{\partial}{\partial \mu}(1-\mu^2)\frac{\partial f}{\partial \mu}\right\}. \quad \text{(A29)}$$

A2.2. Lorentzian Distribution. For a Lorentzian velocity distribution function, the collision term is given by

$$\left(\frac{df}{dt}\right)_c = \sum_\beta 2\pi \frac{Z_\alpha^2 Z_\beta^2 e^4 \ln\Lambda}{m_\alpha^2}\left(\frac{m_\beta}{2kT_\beta}\right)^{3/2} n_\beta \left(\frac{\kappa}{(\kappa-3/2)}\frac{[1-\beta_4(b_2)]}{x^2} \cdot\left\{\frac{1}{x}\frac{\partial^2 f}{\partial x^2} + \frac{1}{x^2}\left[\frac{m_\alpha(2\kappa-3)x^2}{m_\beta\kappa} - 1\right]\frac{\partial f}{\partial x}\right\} + \frac{2A_\kappa}{3\kappa^{3/2}}\left(1+\frac{x^2}{\kappa}\right)^{-\kappa} \cdot\left[\frac{\partial^2 f}{\partial x^2} + \frac{2}{x}\left(1+\frac{m_\alpha}{m_\beta}x^2\right)\frac{\partial f}{\partial x} + 6\frac{m_\alpha}{m_\beta}f\right] + \frac{1}{x^3}\frac{\partial g}{\partial x}\frac{\partial}{\partial \mu}(1-\mu^2)\frac{\partial f}{\partial \mu}\right). \quad \text{(A30)}$$

It can be verified that this expression tends to the expression given by the Maxwellian case when the parameter κ tends to the infinity since

$$\lim_{\kappa\to\infty}\left(1+\frac{x^2}{\kappa}\right)^{-\kappa} \to \exp(-x^2) \quad \text{(A31)}$$
$$\lim_{\kappa\to\infty}(1-\beta_2(b_2)) \to \mathrm{erf(x)} - \frac{2x}{\sqrt{\pi}}e^{-x^2} \quad \text{(A32)}$$
$$\lim_{\kappa\to\infty}(1-\beta_4(b_2)) \to \mathrm{erf(x)} - \frac{2x}{\sqrt{\pi}}e^{-x^2} - \frac{4x^3}{3\sqrt{\pi}}e^{-x^2} \quad \text{(A33)}$$
$$\lim_{\kappa\to\infty}\frac{A_\kappa}{\kappa^{3/2}} \to \frac{2}{\sqrt{\pi}} \quad \text{(A34)}$$

Acknowledgments.
We thank D. Larson for providing us data of electron velocity distribution functions measured by the 3DP instrument on Wind. We also thank the SSTC and P. Simon, Director of IASB/BIRA, for their support.
Michel Blanc thanks Carl Max Hammond Jr. and Oystein Lie-Svendsen for their assistance in evaluating this paper.

References

Barghouthi, I. A., A. R. Barakat, and R. W. Schunk, Monte Carlo study of the transition region in thr polar wind: an

improved collision model, *J. Geophys. Res., 98*, 17583, 1993.

Canuto, C., M.Y. Hussaini, A. Quarteroni, and T. A. Zang, *Spectral Methods in Fluid Dynamics*, Springer-Verlag, New York, 1988.

Chapman, S., and T. G. Cowling, *The Mathematical Theory of Non-uniform Gases*, p.80, Cambridge Univ. Press, New-York, 1970.

Chen, W. M., C. S. Lai, H. E. Lin, and W. C. Lin, Collisionless solar wind in the spiral magnetic field, *J. Geophys. Res., 77*, 1, 1972.

Feldman, W. C., J. R. Asbridge, S. J. Bame, M. D. Montgomery, and S. P. Gary, Solar wind electrons, *J. Geophys. Res., 80*, 4181, 1975.

Hammond, M. C., et al., Variation of electron-strahl in the high-speed solar wind: Ulysses observations, *Astron. Astrophys., 316*, 350, 1996.

Hinton, F. L., Collisional transport in plasma, in *Basic Plasma Physics I and II*, edited by A. A. Galeev and R. N. Sudan, p. 148, North-Holland, New-York, 1983.

Jeans, J. H., *The Dynamical Theory of Gases*, 4th ed., Cambridge Univ. Press, New-York, 1923.

Ko, Y.-K., L. A. Fisk, G. Gloeckler, and J. Geiss, Limitations on suprathermal tails on electrons in the lower solar corona, *Geophys. Res. Lett., 23*, 2785, 1996.

Leblanc, F., and D. Hubert, A generalized model for the proton expansion in astrophysical winds, I, The velocity distribution function representation, *Astrophys. J., 483*, 464, 1997.

Lemaire, J., and M. Scherer, Model of the polar ion-exosphere, *Plant. Space Sci., 18*, 103, 1970.

Lemaire, J., and M. Scherer, Simple Model for an ion-Exosphere in an Open Magnetic Field, *Phys. Fluids, 14*, 8, 1683, 1971a.

Lemaire, J., and M. Scherer, Kinetic models of the solar wind, *J. Geophys. Res., 76*, 7479, 1971b.

Lie-Svendsen, O., and M. H. Rees, An improved kinetic model for the polar outflow of a minor ion, *J. Geophys. Res., 101*, 2415, 1996.

Lie-Svendsen O., V. H. Hansteen and E. Leer, Kinetic electrons in high-speed solar wind streams: Formation of high-energy tails, *J. Geophys. Res., 102*, A3, 4701, 1997.

Lin, R. P., et al., A three-dimensional plasma and energetic particles investigation for the Wind spacecraft, *Space Science Reviews, 71*, 125, 1995.

Maksimovic, M., V. Pierrard and J. Lemaire, A kinetic model of the solar wind with Kappa distributions in the corona, *Astronomy and Astrophysics, 324*, 725, 1997a.

Maksimovic M., V. Pierrard and P. Riley, Ulysses electron distributions fitted with Kappa functions, *Geophys. Res. Let., 24*, 9, 1151, 1997b.

Meyer-Vernet, N., and K. Issautier, Electron temperature in the solar wind: Generic radial variation from kinetic collisionless models, *J. Geophys. Res., 103*, 24,705, 1998.

Ogilvie, K. W. and J. D. Scudder, The radial gradient and collisional properties of the solar wind electrons, *J. Geophys. Res., 83*, 3778, 1978.

Pierrard, V., Fonctions de distribution des vitesses des particules s'échappant de l'ionosphère, Ph.D. thesis, 163 pp., Univ. Catholique de Louvain-La-Neuve, 1997.

Pierrard, V., and J. Lemaire, Lorentzian ion exosphere model, *J. Geophys. Res., 101*, 7923, 1996.

Pierrard, V., and J. Lemaire, A collisional kinetic model of the polar wind, *J. Geophys. Res., 103*, 11,701, 1998.

Pilipp, W. G., et al., Characteristics of electron velocity distribution functions in the solar wind derived from the HELIOS plasma experiment, *J. Geophys. Res., 92*, 1075, 1987.

Rosenbauer, H., et al., A survey of initial results of the HELIOS plasma experiment, *J. Geophys., 42*, 561, 1977.

Schulz, M., and A. Eviatar, Electron temperature asymmetry and the structure of the solar wind, *Cosmic Electrodynamics, 2*, 402, 1972.

Scudder, J. D., On the causes of temperature change in inhomogeneous low-density astrophysical plasmas, *Astrophys. J., 398*, 299, 1992a.

Scudder, J. D., Why all stars should possess circumstellar temperature inversion, *Astrophys. J., 398*, 319, 1992b.

Scudder, J. D., and S. Olbert, A theory of local and global processes which affect solar wind electrons, 1, The origin of typical 1 AU velocity distribution functions: Steady state theory, *J. Geophys. Res., 84*, 2755, 1979a.

Scudder, J. D., and S. Olbert, A theory of local and global processes which affect solar wind electrons, 2, Experimental support, *J. Geophys. Res., 84*, 6603, 1979b.

Shizgal, B., and R. Blackmore, A discrete ordinate method of solution for linear boundary value and eigenvalue problems, *J. Comput. Phys., 55*, 313, 1984.

Spitzer, L., *Physics of Fully Ionized Gases*, 105 pp., Wiley-Interscience, New York, 1956.

Treumann, R. A., Theory of super-diffusion for the magnetopause, *Geophys. Res. Lett., 24*, 1727, 1997.

J. Lemaire and V. Pierrard, Institut d'Aéronomie Spatiale de Belgique, 3 Avenue Circulaire, B-1180, Brussels, Belgium. (e-mail: Joseph.Lemaire@oma.be; viviane@mail.magnet.oma.be)

M. Maksimovic, Space Science Department, European Space Agency, European Space and Technology Center, P.O. Box 299, 2200AG Noordwijk, The Netherlands. (e-mail: mmaksimo@estec.esa.nl)

(Received August 8, 1998; revised December 9, 1998; accepted March 7, 1999.)